




## Open Archive Toulouse Archive Ouverte (OATAO)

OATAO is an open access repository that collects the work of Toulouse researchers and makes it freely available over the web where possible

This is an author's version published in: <http://oatao.univ-toulouse.fr/27621>

**Official URL:** <https://doi.org/10.1016/j.snb.2019.127226>

### **To cite this version:**

Parellada-Monreal, Laura and Gherardi, Sandro and Zonta, Giulia and Malagù, Cesare and Casotti, Davide and Cruciani, Giuseppe and Guidi, Vincenzo and Martínez-Calderón, Miguel and Castro-Hurtado, Irène and Gamarra, Daniel and Lozano, Jesus and Presmanes, Lionel  and Mandayo, Gemma García *WO3 processed by direct laser interference patterning for NO2 detection.* (2020) *Sensors and Actuators B: Chemical*, 305. 127226. ISSN 0925-4005

Any correspondence concerning this service should be sent to the repository administrator: [tech-oatao@listes-diff.inp-toulouse.fr](mailto:tech-oatao@listes-diff.inp-toulouse.fr)

# WO<sub>3</sub> processed by direct laser interference patterning for NO<sub>2</sub> detection

L. Parellada-Monreal<sup>a,b,\*</sup>, S. Gherardi<sup>c</sup>, G. Zonta<sup>c,d</sup>, C. Malagù<sup>c,d</sup>, D. Casotti<sup>d,e</sup>, G. Cruciani<sup>d</sup>, V. Guidi<sup>d,e</sup>, M. Martínez-Calderón<sup>a,b</sup>, I. Castro-Hurtado<sup>a,b</sup>, D. Gamarra<sup>f</sup>, J. Lozano<sup>f</sup>, L. Presmanes<sup>g</sup>, G.G. Mandayo<sup>a,b</sup>

<sup>a</sup> Ceit, Manuel Lardizabal 15, 20018 Donostia/San Sebastián, Spain

<sup>b</sup> Universidad de Navarra, Tecmun, Manuel Lardizabal 13, 20018 Donostia/San Sebastián, Spain

<sup>c</sup> SCENT, S.r.l., Ferrara, Italy

<sup>d</sup> Department of Physics and Earth Science, University of Ferrara, Via Saragat 1/c, 44122 Ferrara, Italy

<sup>e</sup> INFN Section of Ferrara, Via Saragat 1/c, 44122 Ferrara, Italy

<sup>f</sup> Escuela de Ingenierías Industriales, University of Extremadura, Badajoz, Spain

<sup>g</sup> Institut Carnot CIRIMAT, UPS-INPT-CNRS 5085, University Paul Sabatier, Toulouse, France

## ABSTRACT

## ARTICLE INFO

### Keywords:

WO<sub>3</sub>

DLIP

Tetragonal phase

TOP-SIMS

NO<sub>2</sub>

Arrhenius

In this paper two kind of sensors based on WO<sub>3</sub> sputtered by magnetron sputtering and annealed at 600 °C have been studied. The first kind was processed by two-dimensional direct laser interfering patterning (DLIP) and the second one without any additional treatment. Morphological and structural characterization have shown a hole structure in a periodic line-pattern for the DLIP-processed sensors and a flat surface for the only-annealed sensors, both with a tetragonal WO<sub>3</sub> phase. TOF-SIMS analysis has revealed that the first WO<sub>3</sub> layers are reduced for both samples, which could improve sensing performance. Promising response enhancement of DLIP-processed sensors has been observed for low concentrations of NO<sub>2</sub> (from 0.5 ppm to 5 ppm) at 200 °C, lowering the limit of detection (LOD) to 10 ppb, half of the LOD of the only-annealed sensors (20 ppb). Cross sensitivity to CO and HCHO have been investigated and the sensing mechanisms discussed.

## 1. Introduction

In the recent years, special attention has been paid to nanostructured materials for gas sensors, since they open a window of distinctive physical properties for a wide range of materials [1] and the physics behind is based on surface reactions [2,3]. The first chemical sensor based on nanobelts was published in 2002 by the group of Comini [4], showing a new class of stable and very sensitive nanostructured materials for gas detection. The nanostructures preparation methods can tune their structural and morphological characteristics and this allows a controlled modification of the sensor properties and performances [5–8].

Among the preparation methods, the direct laser interference patterning (DLIP) is a good candidate to modify the surface properties of metal oxide semiconductors, enhancing their sensitivity to specific gases. This technique presents some important advantages, since it combines laser heat with interference patterns able to nanostructure areas of about 1 cm<sup>2</sup> in less than a second. Moreover, the nanostructures can be patterned directly on the sensing device (in situ), without the need to transfer them (ex situ), as in the case of many bottom up

techniques.

DLIP was successfully applied to different typologies of materials like semiconductors [9], metals [10] and polymers [11], enhancing their properties for specific applications like doped ZnO for solar cells [12,13], carbon films for tribological applications [14] and graphene oxide for humidity sensors [15].

Previous works show the good sensing capability of WO<sub>3</sub> towards NO<sub>2</sub> gas [16,17], that is one of the most harmful air pollutants as it can cause eye irritation and severe respiratory complications [18,19].

Outdoors NO<sub>2</sub> sources are mainly coming from automotive, chemical industry and it is also present in the acid rain, while home NO<sub>2</sub> sources are gas fueled heating and gas fueled stoves. Nowadays there is not a unanimous agreement on the maximum acceptable levels of NO<sub>2</sub> gas exposure. Nevertheless, the Environmental Protection Agency (EPA) has set 53 parts per billion (ppb) as the highest allowable limit [20] and the World Health Organization (WHO) established that 0.1 ppm of NO<sub>2</sub> limit indoors [19].

Therefore, monitoring very low concentration of NO<sub>2</sub> is crucial to keep under observation its dangerous effects and reduce the impact on the environment and human beings.

\* Corresponding author at Ceit, Manuel Lardizabal 15, 20018 Donostia/San Sebastián, Spain..

E-mail address: lparellada@ceit.es (L. Parellada-Monreal).

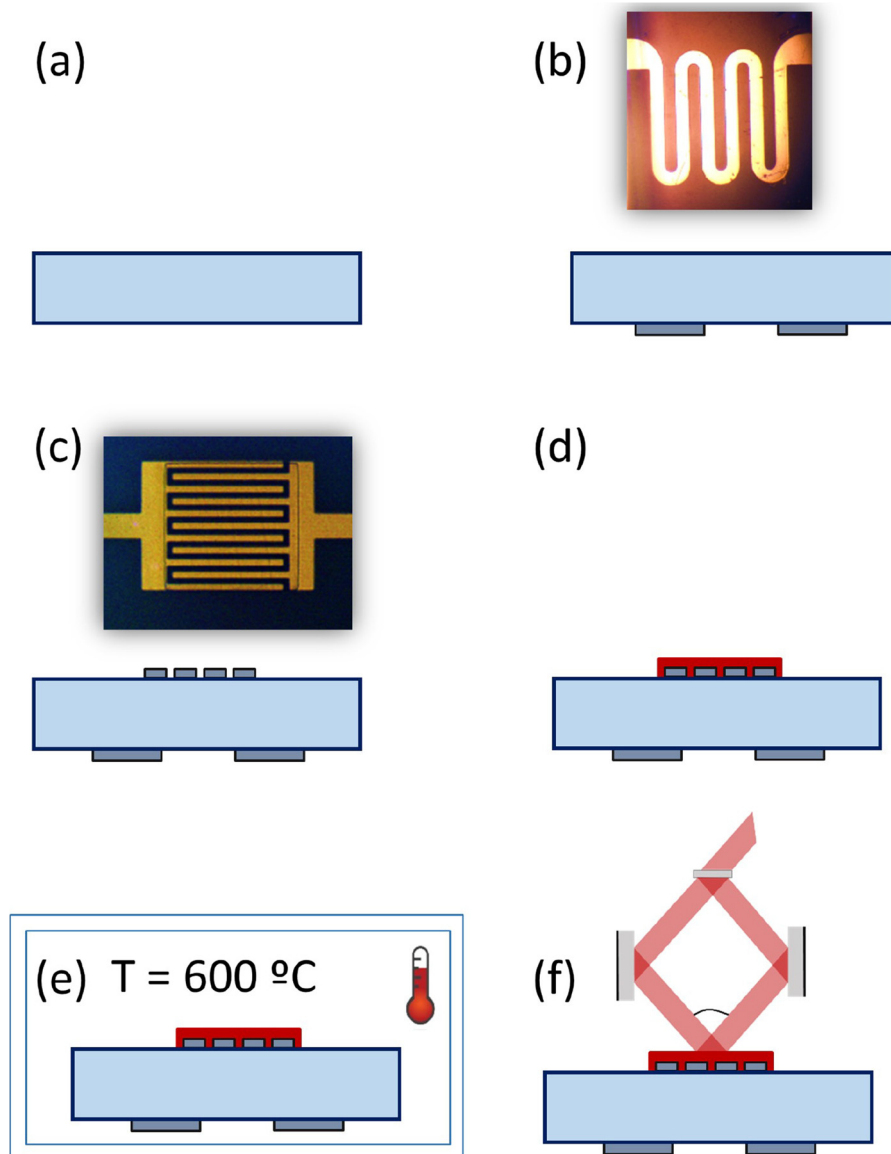


**Fig. 1.** Scheme of the fabrication steps of the  $\text{WO}_3$  sensor device. (a) Polished alumina substrate, (b) DC sputtering Pt heating resistance on the reverse side, (c) DC sputtering IDT electrodes, (d) RF sputtering of  $\text{WO}_3$  sensing layer, (e) thermal annealing at  $600\text{ }^{\circ}\text{C}$  and (f) DLIP processing at  $50\text{ mJ/cm}^2$ .

In this work, both sensing devices, based on  $\text{WO}_3$  thin films annealed at  $600\text{ }^{\circ}\text{C}$  and sensors annealed and processed with a two beam DLIP set up were fabricated and tested with gases. The structural properties of the thin films were characterized by surface and bulk techniques, in order to investigate the laser effect on the devices. Gas sensing performance was investigated for  $\text{NO}_2$  detection. Conductance measurements as a function of temperature were performed in air and  $\text{NO}_2$ , in order to understand the sensing mechanism during detection process of  $\text{NO}_2$ .

## 2. Material and methods

### 2.1. Sensor fabrication

The  $\text{WO}_3$  sensors were fabricated on  $1 \times 2\text{ cm}^2$  polished alumina substrates (Fig. 1 (a)). First of all, a Pt heating resistance was deposited on the reverse side of the alumina substrate shaped by UV photo lithography and grown by DC sputtering in an Edwards ESM 100 system (Fig. 1(b)). The lift off process was carried out with acetone. The same fabrication steps were used to grow Pt interdigitated (IDT) electrodes

for the electrical measurements (Fig. 1(c)). The electrodes have a separation and width of  $50\text{ }\mu\text{m}$ , a length of  $0.9\text{ mm}$  and cover an area of  $1\text{ mm}^2$ . In order to improve the adhesion of the metal to the substrate, a  $25\text{ nm}$  thick Cr layer was deposited under the  $200\text{ nm}$  thick sputtered Pt layer. Afterwards,  $1\text{ mm}^2$   $\text{WO}_3$  sensing layer was deposited on top of the Pt electrodes by photolithography followed by RF reactive magnetron sputtering with a metal oxide target of 99.99% purity. The sputtering process was performed in a Pfeiffer Iontech system at  $300\text{ W}$  of RF power in a mixed atmosphere of oxygen (40%) and argon (60%) and under  $5 \times 10^{-3}$  mbar of pressure. The sputtering time was 1 h, the deposition temperature was between  $25\text{ }^{\circ}\text{C}$  and  $30\text{ }^{\circ}\text{C}$  and as for the Pt, acetone was used for the lift off process (Fig. 1(d)). Finally, the sensor device was thermally stabilized in a quartz oven at  $600\text{ }^{\circ}\text{C}$  during 4 h in synthetic air (Fig. 1(e)). The only annealed samples were labelled TT600C. The annealing temperature was chosen considering previous results obtained by our research group [21].

After annealing, some sensors were processed by two beam DLIP set up with a frequency tripled Q switched Nd:YAG laser source provided by Thales, the Saga HP model (with a wavelength of  $355\text{ nm}$ , a pulse duration of  $8\text{ ns}$ , a maximum energy of  $600\text{ mJ}$  per pulse and a

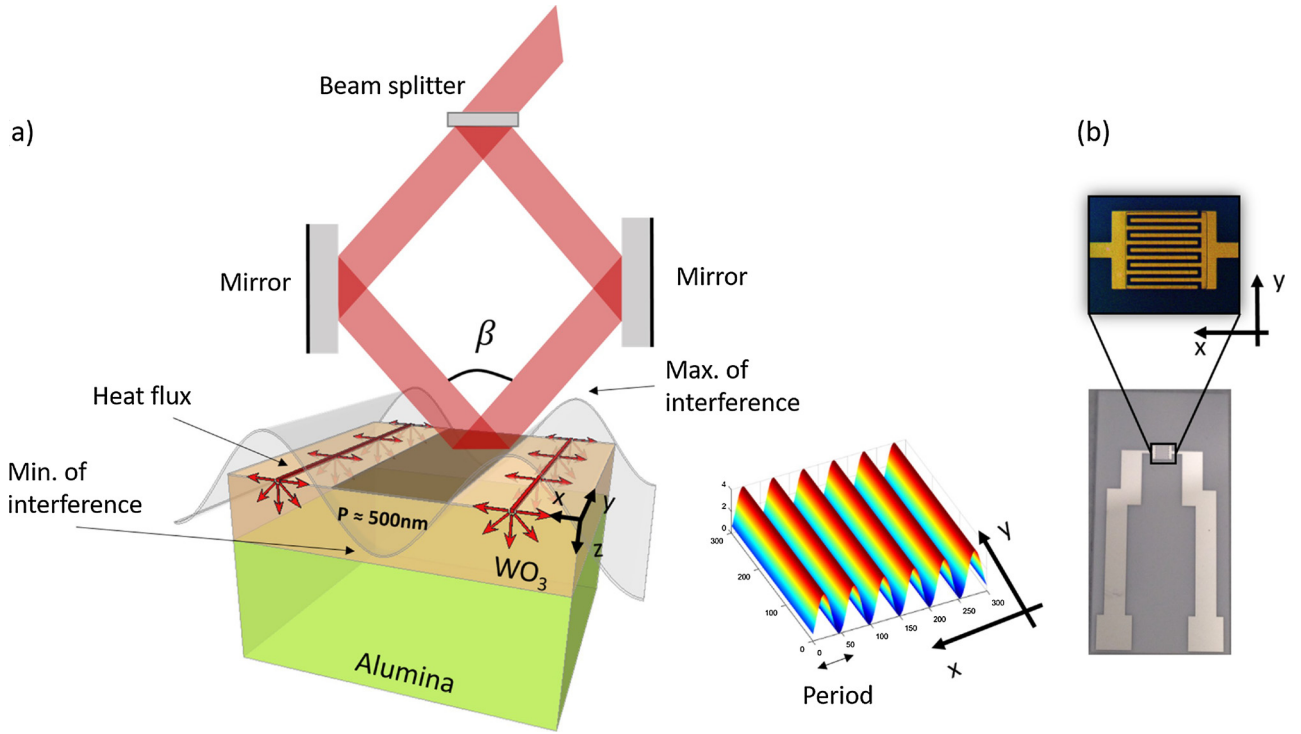


Fig. 2. (a) Schematic two-beam DLIP set-up processing  $\text{WO}_3$  thin film on alumina and an energy distribution simulation of one-dimensional pattern. (b) Detailed image of the IDT electrodes with the coordinates, indicating that the maximum and minimum of interference are perpendicular to the electrodes.

flat top energy distribution) to obtain one dimensional interference patterns on the surface (see Fig. 1(f)). The interference patterns are a distribution of maximum and minimum intensity peaks, that lead to nanostructures down to a fraction of the laser wavelength. The areas of the material exposed to higher intensities than its ablation or annealing threshold are morphologically and structurally modified, getting melted or even removed, while areas exposed to lower intensities than these thresholds remain unaffected.

A detailed schematic drawing of the set up is shown in Fig. 2: an optical beam splitter divides the laser source into two different beams; afterwards they are reflected in mirrors and finally addressed towards the sample surface with the same incident angle. The maximum and minimum of interference are indicated with a sinusoidal wave and the heat flux generated by the laser is indicated with red arrows. An example of a typical energy distribution of two beam configuration DLIP is also shown. The maximum and minimum of interference are perpendicular to the IDT electrodes, as indicated by the coordinates in Fig. 2(b).

The period of the structure ( $P$ , distance between two maxima or two minima of interference) is defined by the angle between the two laser beams ( $\beta$ ) and the wavelength ( $\lambda$ ):

$$P = \frac{\lambda}{2 \sin \frac{\beta}{2}} \quad (1)$$

In order to fabricate lines with a theoretical period of 500 nm, an angle of  $41.5^\circ$  was set up. The necessary fluence to obtain one dimensional interference patterns on the surface of  $\text{WO}_3$  thin film annealed at  $600^\circ\text{C}$ , was found to be optimum for a value of  $50 \text{ mJ}/\text{cm}^2$  with a single shot. Samples processed at lower fluences than  $50 \text{ mJ}/\text{cm}^2$  did not present any morphological modification. The DLIP processed samples were labelled TT600C + DLIP50.

## 2.2. Film characterization

For the  $\text{WO}_3$  film characterization, samples with a size of  $6 \times 7 \text{ mm}^2$

were fabricated by sputtering and annealed at  $600^\circ\text{C}$  following the same recipe as in previous section. Some samples have been also processed by DLIP, as explained in the sensor fabrication section.

The film thickness was determined by a KLA Tencor Profiler, resulting in an average thickness of 145 nm.

Regarding the morphological characterization, JPK Nanowizard 3 atomic force microscope (AFM) was employed. Tapping mode images were obtained using silicon Tap300 G cantilevers with a resonance frequency around 300 kHz. The tip radius is smaller than 10 nm and the half cone angle is around  $25^\circ$ .

A scanning electron microscopy (SEM) Quanta 3D FEG from FEI Company was used to study the homogeneity of the DLIP process in the sample as well as for a cross section analysis.

The X ray diffraction analysis was performed by a Bruker D8 Advance diffractometer in grazing incident (GIXRD) configuration ( $1.8^\circ$  incident angle). The diffractometer was equipped with a copper X ray tube operating at 40 kV and 40 mA, and with a LYNXEYE XE detector. Samples were placed on a quartz zero background holder. Measuring conditions were  $5-80^\circ 2\theta$  range,  $0.02^\circ 2\theta$  scan rate, and 0.8 s per step of counting time. The mean crystallites size, the strain of the crystallites and the cell parameters were determined by whole profile fitting Powley and Le Bail methods [22,23] as implemented in the TOPAS v 4 program by Bruker AXS [24]. The fundamental parameters approach was used for the line profile fitting [25-27]. In this approach, the instrumental component of peak broadening is calculated by the convolution of instrument profile functions for optics and X ray tube emission. Thus, the sample components to peak broadening (crystallite size and strain) are the only peak shape parameters to be optimized in the profile fitting procedure. In particular, the Double Voigt method [28] implemented in TOPAS allowed to calculate the crystallite size and strain as volume weighted for the mean column heights based on the sample dependent integral breadths of peaks.

Raman spectra were collected under ambient conditions using Horiba Jobin Yvon LabRAM HR 800 spectrometer equipped with a fiber coupled 532 nm laser. Spectra acquisition was carried out using a  $\times 100$  objective lens and 1800 g/mm grating. During the measurement, the

resulting laser power at the surface of the sample was adjusted to 4 mW. Exposure time ranged from 100 to 200 s.

The composition depth profile of different ions was measured using a time of flight secondary ion mass spectrometer (TOF-SIMS 5, ION TOF). The mass spectrum was obtained by measuring the time of flight distribution of the positive ions coming from the sample surface into the detector. The primary ions source was Bi<sup>+</sup> operating at 25 keV and the spot size for the depth profile was 50 μm × 50 μm. Sputtering was done using 1 keV oxygen beam over a 300 μm × 300 μm of raster size area.

### 2.3. Electrical characterization

The response of the sensors was carried out by flowing the gases, controlled by mass flow controllers (MFC), into two cylindrical aluminum chambers of 600 and 10.8 ml.

The larger chamber was used to test the sensors at different temperatures (150–400 °C) for 5 ppm of NO<sub>2</sub>. At the optimal temperature, lower NO<sub>2</sub> concentrations were tested, as well as NO<sub>2</sub> mixtures with CO and HCHO. The total flux into the chamber was set at 500 sccm and the uniformly gas distribution was guaranteed by a diffuser placed at the bottom of the chamber with holes disseminate at its surface.

The small chamber was used to perform the Arrhenius plots, following the steps below reported:

- (i) In 400 sccm of air, the sensor was heated to 450 °C in less than 30 min and left for 10 min.
- (ii) The sensor was cooled down to ~100 °C and after a minute, the temperature was increased up to ~500 °C with steps of ~5 °C/min.
- (iii) The same procedure was performed in 5 ppm of NO<sub>2</sub>.

The NO<sub>2</sub>, CO and HCHO gases were taken from certified bottles mixed with synthetic air (Air Liquide). The circuit used to measure the sensors conductance in the presence of gas includes an inverting operational amplifier (OA) (see Fig. S1 in the Supporting Information).  $R_s$  and  $R_f$  are the sensor and the reference resistance, respectively.  $R_f$  can be freely modified and must be in the same order of magnitude as  $R_s$ . As  $V_{in}$  and  $R_f$  are known and constant, the output voltage,  $V_{out}$ , is proportional to the conductance of the sensor,  $G$ , as indicated in Eq. (2):

$$V_{out} = -\frac{R_f}{R_s} \cdot V_{in} = \text{const.} \cdot G \quad (2)$$

The output voltage is measured through a Keithley 2000 Multimeter connected via GPIB to the computer, where a Labview© is acquiring the data.

The power consumption of the Pt heating element was doubly calibrated with a thermographic camera and a Pt100 resistance, so the heater is power controlled by a voltage source. Information regarding the calibration is introduced in the Supporting Information.

In this work, the response of the devices, SR, is defined as Eq. (3):

$$SR = G_{air}/G_{gas} \quad (3)$$

where  $G_{air}$  is the conductance of the sensor in air (baseline), and  $G_{gas}$  represents the sensor conductance after 30 min of gas exposure. The recovery time is defined as the time elapsed until the 10% of the initial baseline resistance is reached after the gas extraction.

## 3. Characterization results

### 3.1. Morphological and structural characterization

The AFM image of Fig. 3(a) shows a flat surface for the sample thermal annealed WO<sub>3</sub> at 600 °C with a root mean square (RMS) roughness of 7 nm, while for the DLIP processed sample (Fig. 3(b) and (d)) a hole structure appears in a periodic line pattern. The RMS roughness, as the average between the processed and non processed

regions, has increased to values between 10 and 15 nm. The profile section of the DLIP processed sample measured from the AFM images (Fig. 3(c)) indicates that the average depth of the holes is 18 nm. Nevertheless, from the cross section images performed by FIB (Fig. 4), the hole structure seems to be reaching the substrate, so probably the profile sections of Fig. 3(c) are underestimating the depth due to the high half cone angle of the tip.

The line patterned morphology indicates that the hole area corresponds to the places where higher intensity has been accumulated and consequently a higher temperature has been reached, melting material. Precisely, the highest area around the holes (Fig. 3(d)) seems to be the melted WO<sub>3</sub> moved from inside the cavities, as explained by the Marangoni convection mechanism [29].

From the SEM images (see S1 in the supporting information), a bigger area of the nanostructured sample can be analysed, showing a great homogeneity of the nanostructuring with the desired period.

Many polymorphic structures have been identified in WO<sub>3</sub> as a function of temperature [30–34]: monoclinic (for temperatures lower than –50 °C and from 17 °C to 330 °C), triclinic (from –50 °C to 17 °C), orthorhombic (from 330 °C to 740 °C) and tetragonal (for temperatures higher than 740 °C). Not all the transitions are reversible and the lattice constants of each crystal structure can be found in [35]. The sensing performance is expected to be affected by the crystal structure as shown by I. M. Szilágyi et. al., who found that monoclinic WO<sub>3</sub> shows good selectivity to H<sub>2</sub>S, while hexagonal WO<sub>3</sub> sensors present lower sensitivity but much faster response [36].

The GIXRD patterns of the as grown, only annealed (TT600C) and DLIP processed (TT600C + DLIP50) samples are reported in Fig. 5. All patterns show peaks corresponding to the alumina substrate (space group R $\bar{3}c$ , PDF 010 0173). The as grown sample does not show peaks attributable to any WO<sub>3</sub> crystalline structure, while the only annealed and DLIP processed samples show peaks belonging to the tetragonal WO<sub>3</sub> structure (space group  $P4/nmm$ , PDF 018 1417), but the relative intensity of the (110) peak does not match the PDF data for powder tetragonal WO<sub>3</sub> structure, indicating that in both samples the crystallites grow with significant preferential orientation. This result is in agreement with previous investigations [21] and indicates that the laser modifications does not destabilize the tetragonal crystal structure. The stability of the crystal structure and the crystal size are important issues for the sensing mechanism [37].

Table 1 reports the cell parameters, the mean crystallites size and microstrain of the crystalline samples. Cell parameters and strain, that were calculated by Powley and Le Bail methods, are also very similar for both the samples treated and not treated with laser. Nevertheless, even if it remains within the error bars, a slight increase of the crystallite size of the DLIP processed sample compared to only annealed WO<sub>3</sub> has been observed.

Tetragonal phase of WO<sub>3</sub> is expected to appear for temperatures higher than 740 °C in bulk WO<sub>3</sub> [34] and the annealing performed in this work is at 600 °C. Nevertheless, in structures with nanometric crystals, as it is the case of the samples here, temperature and pressure of phase transitions can be strongly modified. A downshift in temperature for the tetragonal transition is shown in [38] for crystal sizes between 16 and 60 nm and the samples analysed here are in this range, as shown in Table 1.

Raman spectra (see Fig. 6) supports the above considerations. The as grown samples only show peaks coming from the alumina substrate [39] (highlighted with an asterisk in Fig. 6) while both samples types (only annealed and DLIP processed) present the same WO<sub>3</sub> Raman modes for the measured spectra.

The peaks coming from the WO<sub>3</sub> thin film are found at 267.7, 692.1 and 802.4 cm<sup>-1</sup>. As it is known, the peaks at low frequencies (200–500 cm<sup>-1</sup>) correspond to bending vibrations, while the high frequency ones that appear at frequencies between 600 and 1000 cm<sup>-1</sup> are stretching modes [40]. Therefore, the lowest peak can be associated to a bending mode  $\delta(\text{O W O})$  [41] and the peaks in the range of

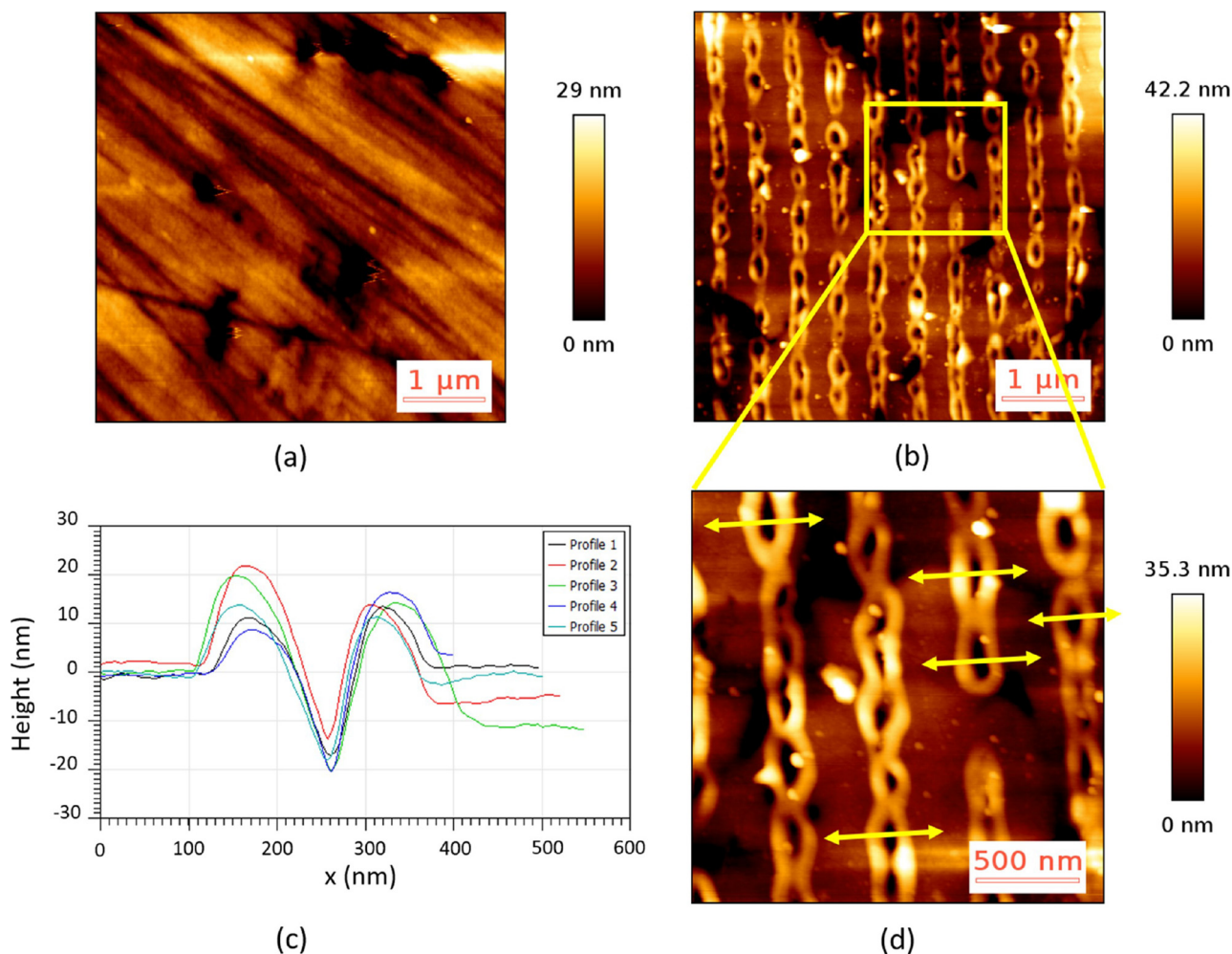


Fig. 3. AFM tapping mode images of  $\text{WO}_3$  thin film (a) only-annealed and (b) DLIP-processed. (c) Profiles of the sections point out in (d); (d) zoomed image of the sample DLIP-processed.

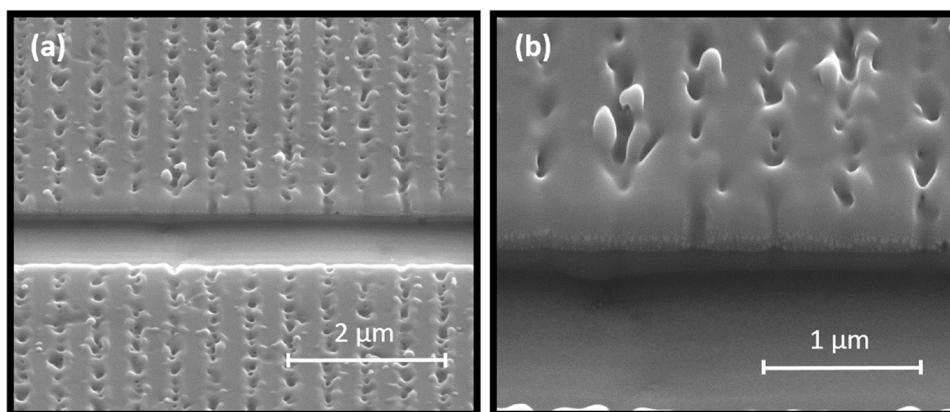


Fig. 4. (a) SEM image of a cross-section of the sample DLIP-processed and (b) a zoom SEM image of (a).

$700\text{--}800\text{ cm}^{-1}$  are related to stretching modes  $\text{O W O}$  [42] and  $\text{W}^{6+}\text{ O}$  [41], respectively.

### 3.2. TOF SIMS characterization

Positive TOF SIMS in depth experiments were performed to analyse the qualitative composition of the samples as a function of thickness. The detected ions related to  $\text{WO}_3$  were  $\text{W}^+$ ,  $\text{WO}^+$  and  $\text{WO}_2^+$  and the alumina related ions detected were  $\text{Al}^+$  and  $\text{AlO}^+$ .

The measurements were performed twice at different sample areas with high repeatability of the results. In Fig. 7, only  $\text{AlO}^+$  (for alumina) and  $\text{W}^+$ ,  $\text{WO}^+$  and  $\text{WO}_2^+$  ions (for  $\text{WO}_3$ ) of one of the measurements have been plotted, representing the sample behaviour. The signals shown in Fig. 7 have been filtered in order to reduce the noise generated by the equipment. The steeply increase in the intensity for the ion  $\text{WO}_2^+$  in the as grown sample and the slow decrease of  $\text{W}^+$  indicate that the sample is getting more oxidized as a function of the  $\text{WO}_3$  sample depth. By contrast, in the other two samples, only a slight increase of

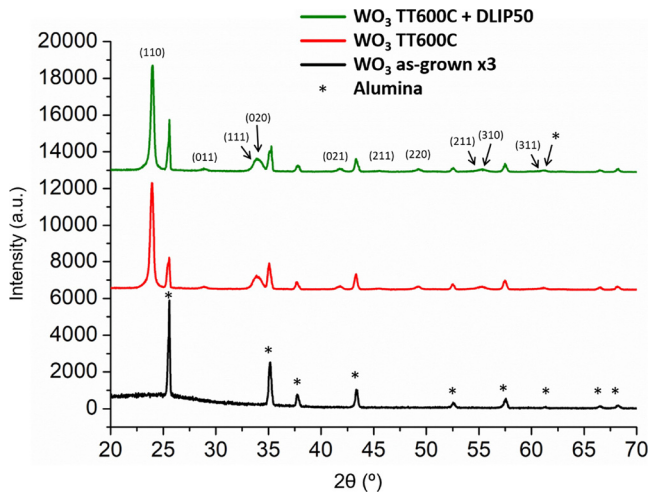


**Fig. 5.** GIXRD measurements of the WO<sub>3</sub> thin film as-grown, WO<sub>3</sub> only-annealed and WO<sub>3</sub> DLIP-processed. All patterns show peaks of the Al<sub>2</sub>O<sub>3</sub> substrates marked with \*, the other peaks are attributable to WO<sub>3</sub> tetragonal phase.

**Table 1**

Cell parameters, mean crystallite size and microstrain calculated by Le Bail and Powley methods for the two different samples.

Method	Parameters	WO <sub>3</sub> TT600C	WO <sub>3</sub> TT600C + DLIP50
Le Bail	a (Å)	5.2288(2)	5.2288(2)
	c (Å)	3.7963(6)	3.7974(8)
	Size (nm)	47(3)	51(5)
	Strain	0.24(1)	0.24(1)
Powley	a (Å)	5.2286(2)	5.2287(3)
	c (Å)	3.7955(7)	3.7967(9)
	Size (nm)	44(3)	49(6)
	Strain	0.23(1)	0.23(2)

the WO<sub>2</sub><sup>+</sup> and a decrease of W<sup>+</sup> before stabilization is shown. This result means that the first layers of the WO<sub>3</sub> are reduced, compared to the rest of the thin film and this could be explained by the existence of oxygen vacancies. As it is known, surface defects promote the gas detection and specially oxygen vacancies have been widely investigated as they increase the adsorption of gas molecules [43,44,7,45,46]. Moreover, the intensities of WO<sup>+</sup> and WO<sub>2</sub><sup>+</sup> ions are more parallel for the WO<sub>3</sub> DLIP

processed thin film, compared to only annealed one (see Fig. 7(b) and (c)). This can be originated by a higher homogeneity degree.

The sputter rate during the TOF SIMS measurements has been calculated taking into account the WO<sub>3</sub> thickness deduced from cross sections observed by SEM. A small increase of the sputter rate is observed comparing the as grown with the only annealed and DLIP processed sample (see Table 2). This could be due to the increase of the homogeneity of the laser treated sample that raises the sputter velocity. The interface region between the thin film and the WO<sub>3</sub> is also shown in Table 2 and indicated in garnet in Fig. 7. As it is expected, the interface region increases significantly with the annealing (62.9 nm) compared to as grown (39.8 nm), because the atoms receive more energy. Therefore, a slight inter diffusion can occur at the interface between the WO<sub>3</sub> layer and the alumina substrate. In the case of the sample also treated by DLIP, even a larger interface region (75.2 nm) is shown. This is explained by the higher temperatures (around 1000 K) that the sample reaches with the laser shot, although the shot time is in the nanosecond scale. Similar results were found for ZnO processed by DLIP at different fluences [9].

It is well known that the diffusivity has a great role on the sensitivity and the response time as demonstrated by G. Sakai et al. [47]. The surface patterned by DLIP has clearly a higher surface to volume ratio due to the holes generated in the thin film that should improve the gas diffusion. However it remains difficult to measure such surface enhancement factor since the size of the samples is much too small to be able to carry out surface measurements by gas adsorption [48].

#### 4. Sensor results and discussion

Due to the importance of the working temperature during the gas detection, the response to 5 ppm of NO<sub>2</sub> at different stationary temperatures (150 400 °C) is reported in Fig. 8. Two sensors of each type are plotted, showing a good reproducibility between sensors of the same type. At temperatures ≥ 250 °C, DLIP processed sensors respond to NO<sub>2</sub> by decreasing their conductivity but with a very low response, between 1.18 and 1.58. By contrast, sensors only annealed at 600 °C do not detect NO<sub>2</sub> for these temperatures or increase their conductivity (although the conductivity is increasing, the response is calculated through Eq. (3) because NO<sub>2</sub> is an oxidizing gas). The values of the response for only annealed sensors at temperatures ≥ 250 °C range from 1.03 to 0.55.

For temperatures lower than 250 °C, the response of both sensors

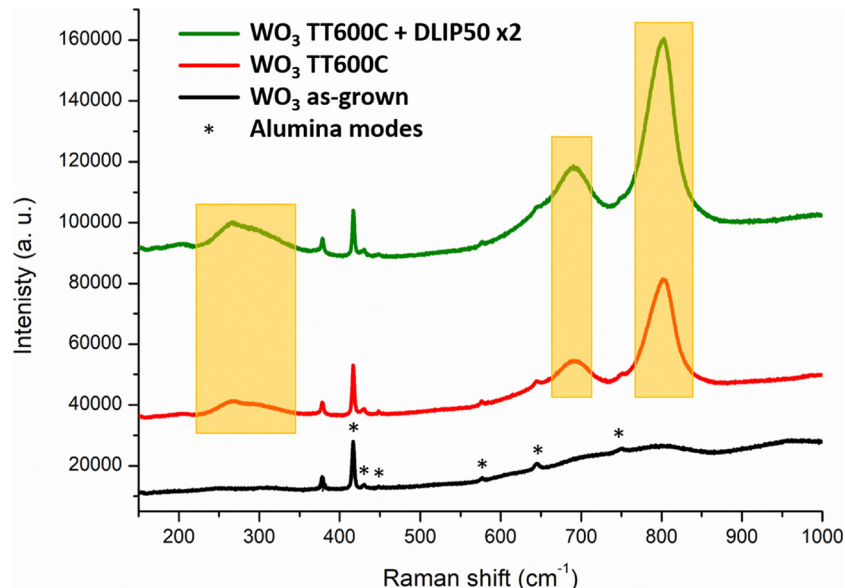
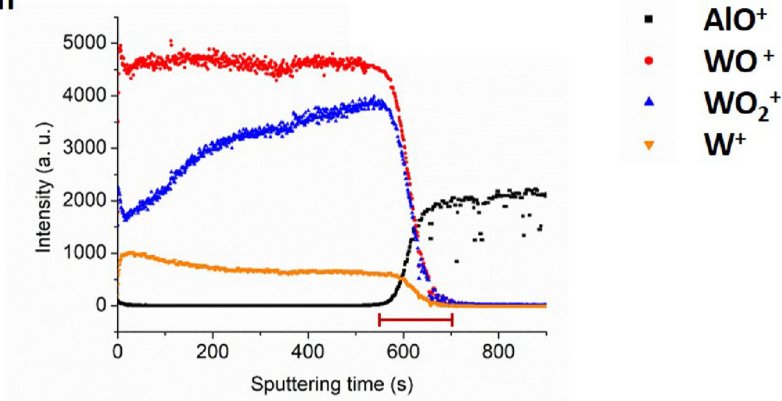
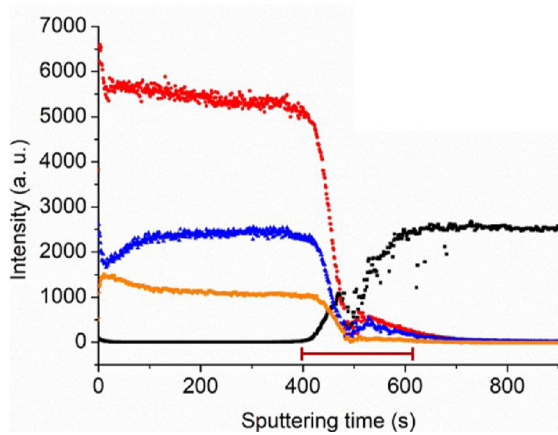


**Fig. 6.** Raman spectra of the WO<sub>3</sub> thin film as-grown, WO<sub>3</sub> only-annealed and WO<sub>3</sub> DLIP-processed.

(a) WO<sub>3</sub> as-grown



(b) WO<sub>3</sub> TT600C



(c) WO<sub>3</sub> TT600C + DLIP50

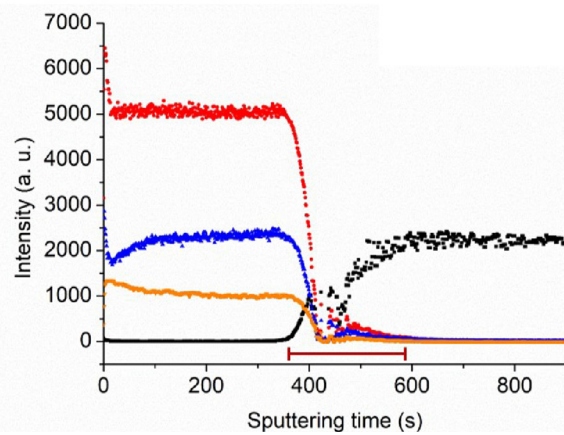


Fig. 7. TOF-SIMS measurements of AlO<sup>+</sup>, WO<sup>+</sup> and WO<sub>2</sub><sup>+</sup> ions for the samples (a) WO<sub>3</sub> as-grown, (b) WO<sub>3</sub> only-annealed and (c) WO<sub>3</sub> DLIP-processed.

Table 2

Sputter rate during the TOF-SIMS measurements and interface region between the alumina and the thin film of the WO<sub>3</sub> as-grown, WO<sub>3</sub> only-annealed and WO<sub>3</sub> DLIP-processed.

Sample	Sputter rate (nm/s)	Interface region (nm)
As-grown	0.22	39.8
WO <sub>3</sub> TT600C	0.27	62.9
WO <sub>3</sub> TT600C + DLIP50	0.32	75.2

increases while decreasing the temperature, but DLIP processed sensors present responses  $\approx 3.5$  times higher than only annealed sensors. Due to the long recovery time at 150 °C (48 min for only annealed sensors and 13 min for DLIP processed sensors), the chosen optimal temperature was 200 °C for both sensors, where the recovery times were decreased to 10 and 7 min, respectively.

The sensitivity of the sensors at the optimal temperature was studied by the response obtained at different NO<sub>2</sub> concentrations (Fig. 9(a)). From the sensitivity graph (see Fig. 9(b)), two different slopes can be observed for concentrations higher and lower than 2 ppm. The average sensitivity values obtained for higher concentrations are 1.74 and 0.47 ppm<sup>-1</sup> for DLIP + TT600C and TT600C, respectively. Nevertheless, for the lower ones, the sensitivity values of both sensor type decrease to 0.95 and 0.20 ppm<sup>-1</sup> for DLIP + TT600C and TT600C, respectively, but the reproducibility of the sensors is higher.

The limit of detection (LOD) has been calculated using the following approximation, as reported in [49]:  $LOD = 3\sigma/b$ , where  $\sigma$  is the standard deviation of the baseline during 5 min and  $b$  is the slope of the sensitivity curve in the concentration range of 0.5–2 ppm. Nevertheless,

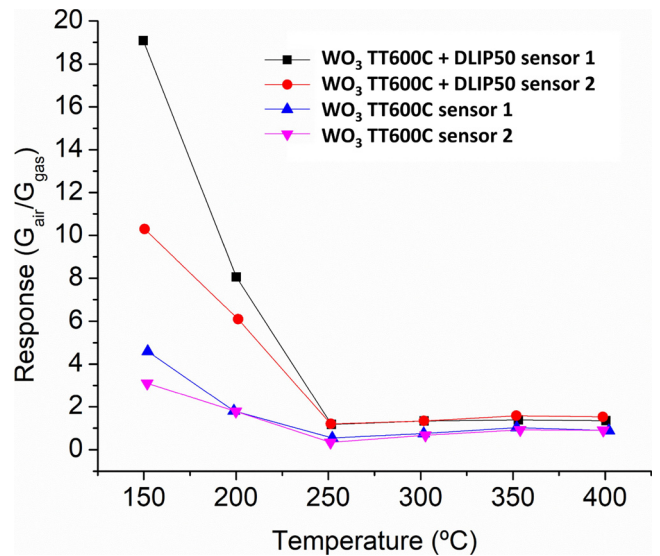


Fig. 8. Response as a function of temperature for 5 ppm of NO<sub>2</sub> for two sensors DLIP-processed and two sensors only-annealed.

in order to give an exact value of the LOD, measurements with ppb levels of NO<sub>2</sub>, such as the reported in [50] should be performed. The results show that in the sensors processed by laser (LOD = 10 ppb), the LOD decreased to half of the value of only annealed samples (LOD = 20 ppb).

In order to study the cross sensitivity, mixtures of some interfering



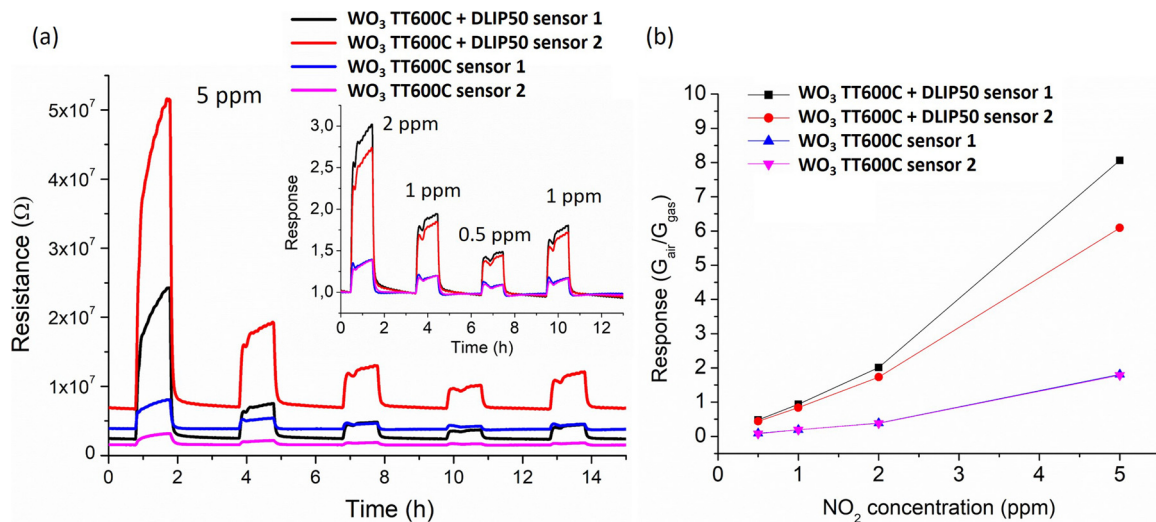


Fig. 9. (a) Resistance variation of two sensors DLIP-processed and two sensors only-annealed for 5, 2, 1, 0.5 and 1 ppm of NO<sub>2</sub> at 200 °C. Response of the low concentrations are shown as an inset. (b) Sensitivity of the different sensors at 200 °C for concentrations between 0.5 and 5 ppm of NO<sub>2</sub>.

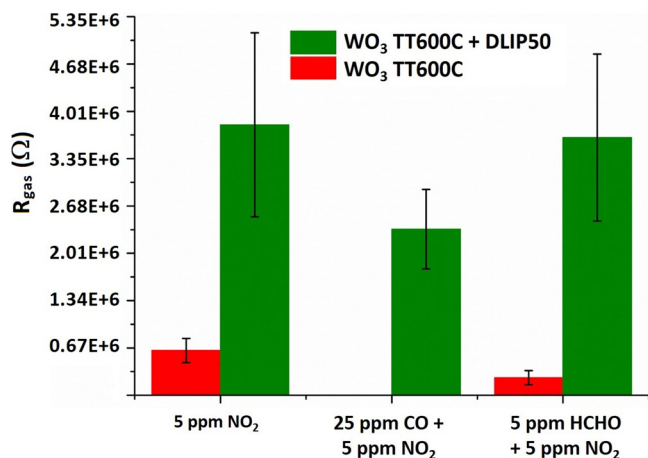


Fig. 10. Responses at 200 °C for 5 ppm of NO<sub>2</sub>, 5 ppm of HCHO + 5 ppm of NO<sub>2</sub> and 25 ppm of CO + 5 ppm of NO<sub>2</sub>.

gases with 5 ppm of NO<sub>2</sub> have also been tested at 200 °C, as shown in Fig. 10 (the error bars of the final resistance values have been calculated with the data of two different sensors). Common concentrations of interest for the interfering gases have been chosen: 25 ppm of CO and 5 ppm of HCHO. The results show that the NO<sub>2</sub> oxidizing contribution is dominant, overcoming the reducing interference, especially for the DLIP processed sensors. The performance of DLIP processed sensors makes them suitable to be employed as NO<sub>2</sub> sensors in atmospheres with CO and HCHO.

As shown in the previous section, significantly different responses have been found for the two type of sensors tested in the experimental conditions considered in the present work. Therefore, different detection mechanisms can be suggested in the two cases.

For low temperatures ( $T < 250$  °C) it is generally accepted that reaction (4) takes place, where NO<sub>2</sub> reacts directly with the semiconductor surface, generating adsorbed NO<sub>2</sub> species and, consequently, decreasing the conductivity of the material [51–53].



At higher temperatures, the reducing behaviour of NO<sub>2</sub> has also been reported for WO<sub>3</sub> based sensors [54], as in the current case for the only annealed sensors. It is accepted that NO<sub>2</sub> gas is adsorbed on the WO<sub>3</sub> surface forming nitrito type adsorbates (ONO<sup>-</sup>) that after dissociate into nitrosyl type adsorbates (NO<sup>-</sup>, NO<sup>+</sup>). The reducing

response observed for temperatures above 250 °C might be due to superior number of NO<sup>+</sup> adsorbates than NO<sup>-</sup> [54].

According to the work of Yamazoe et al. [55], in the case of oxidizing gases and especially for NO<sub>2</sub> it had been demonstrated that a shielding effect can occur due to the oxygen contained in the background gas. In this case the power law is no more effective for very low NO<sub>2</sub> concentrations. The determination of the LOD by extrapolating the sensitivity curve to very low NO<sub>2</sub> concentration could therefore be not accurate and it would be better to make the measurements at low concentrations.

At 200 °C, the main difference between the detection mechanism of reducing and oxidizing gases is that while reducing gases interact with the adsorbed oxygen species, oxidizing agents such as NO<sub>2</sub> tend to be directly adsorbed on the surface (reaction (4)). On WO<sub>3</sub> material is difficult to absorb oxygen in an active form such as O<sup>-</sup> and consequently the reducing agents (CO and HCHO) do not strongly modify the NO<sub>2</sub> response, leading to good selectivity to the oxidizing gas, specially for DLIP processed sensors.

In order to understand the oxygen species adsorbed in each type of sensor, the conductance has been measured as a function of the temperature as described in the experimental section. The Arrhenius plot in air and under 5 ppm of NO<sub>2</sub> are shown in Fig. 11. The method and analysis proposed by Lantto in [56] have been used to interpret the Arrhenius plot results obtained. This method relates the shape and slopes of the Arrhenius plots under different oxygen concentrations to the oxygen species adsorption. As it is also explained in [57,58], the minimum in resistance (or maximum in conductivity) at low temperatures, in the conductance variation in air, is where the O<sup>-</sup> adsorption starts counteracting the O<sub>2</sub><sup>-</sup> adsorption, as can be seen in Fig. 11. The difference between conductivity curves in air and in air with 5 ppm of NO<sub>2</sub> (looking at the range from 150 °C to 250 °C) is bigger for the DLIP processed sensors, which may also be related to the fact that the DLIP processed sensors present higher response to NO<sub>2</sub>. From Fig. 11, it can be appreciated that the slopes before and after the maximum in conductance for the DLIP processed sensors are steeper than for only annealed sensors, indicating that laser treated sensors present higher concentration of sites for adsorption or physisorption. This result highlights that the DLIP processed sensors probably have laser induced defects that work as adsorption sites, apart from the oxygen vacancies revealed by TOF SIMS. This would enhance the NO<sub>2</sub> sensitivity, since more NO<sub>2</sub> molecules could be adsorbed, extracting electrons from the conduction band and thus increasing the resistance.

In fact, we consider that the conduction in tungsten oxide is mainly

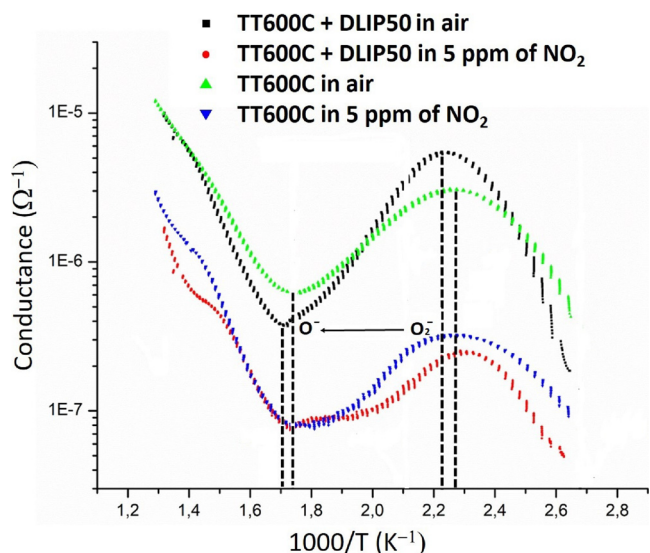


Fig. 11. Arrhenius plots in air and in 5 ppm of NO<sub>2</sub> for the sensors only-annealed and DLIP-processed.

due to the oxygen vacancies with a contribution of the adsorbed oxygen, as shown by the different responses to oxidizing and reducing agents. In [59], the authors study the conductivity of sputtered and thermal evaporated WO<sub>3</sub>, whose morphology is similar to the reported in our study. In fact, the shape of the Arrhenius plot they present shows in similar experimental conditions shows correspondence to the reported in our study, with maxima and minima at similar temperatures.

## 5. Conclusions

One dimensional structures have been generated by DLIP technique on WO<sub>3</sub> thin film sensors after annealing and compared to only annealed sensors. The surface morphology modification has not affected the crystal structure, which remains tetragonal for both films, with similar crystallite sizes. Raman characterization confirms the good crystalline structure of the WO<sub>3</sub> and TOF SIMS analysis shows reduced layers on the top of the WO<sub>3</sub> film, probably due to oxygen vacancies.

Sputtered WO<sub>3</sub> based sensors processed by DLIP have shown responses  $\approx$  3.5 times higher than only annealed sensors to NO<sub>2</sub> at 200 °C. The LOD is 20 ppb for the only annealed sensors and it decreases to 10 ppb for the DLIP processed sensors. Besides, DLIP processed sensors show low cross sensitivity to CO and HCHO, that makes them suitable for environmental applications.

Conductance variation as a function of temperature in air atmosphere and under 5 ppm of NO<sub>2</sub> points out that DLIP processed sensors probably present a higher number of adsorption sites. This contributes to the enhancement of the NO<sub>2</sub> sensitivity.

## Acknowledgements

This work was supported by the Ministry of Economy and Competitiveness (MINECO) through the TEMIN AIR+ (project n<sup>o</sup>. TEC2016 79898 C6 3 R) and by the Basque Government under the Elkartek program (MICRO4FAB grant n<sup>o</sup>. KK 2016 00030). All the authors thank the technical and human support provided by Facility of Analysis and Characterization of Solids and Surfaces of SAIUEx UEX for the TOF SIMS and SEM measurements. The authors also wish to thank SCENT s. r. l. for financing this research.

## Appendix A. Supplementary data

Supplementary data associated with this article can be found, in the

online version, at <https://doi.org/10.1016/j.snb.2019.127226>.

## References

- [1] G. Jimenez-Cadena, J. Riu, F.X. Rius, Gas sensors based on nanostructured materials, *Analyst* 132 (11) (2007) 1083–1099.
- [2] S.R. Morrison, Semiconductor gas sensors, *Sens. Actuators* 2 (1981) 329–341.
- [3] C. Wang, L. Yin, L. Zhang, D. Xiang, R. Gao, Metal oxide gas sensors: sensitivity and influencing factors, *Sensors* 10 (3) (2010) 2088–2106.
- [4] E. Comini, G. Faglia, G. Sberveglieri, Z. Pan, Z.L. Wang, Stable and highly sensitive gas sensors based on semiconducting oxide nanobelts, *Appl. Phys. Lett.* 81 (10) (2002) 1869–1871.
- [5] Y.-F. Sun, S.-B. Liu, F.-L. Meng, J.-Y. Liu, Z. Jin, L.-T. Kong, J.-H. Liu, Metal oxide nanostructures and their gas sensing properties: a review, *Sensors* 12 (3) (2012) 2610–2631.
- [6] L. Zhang, J. Zhao, J. Zheng, L. Li, Z. Zhu, Shuttle-like ZnO nano/microrods: facile synthesis, optical characterization and high formaldehyde sensing properties, *Appl. Surf. Sci.* 258 (2) (2011) 711–718 doi:10.1016/j.apsusc.2011.07.116.
- [7] M. Chen, Z. Wang, D. Han, F. Gu, G. Guo, Porous ZnO polygonal nanoflakes: synthesis, use in high-sensitivity NO<sub>2</sub> gas sensor, and proposed mechanism of gas sensing, *J. Phys. Chem. C* 115 (26) (2011) 12763–12773.
- [8] Z. Liu, M. Miyauchi, T. Yamazaki, Y. Shen, Facile synthesis and NO<sub>2</sub> gas sensing of tungsten oxide nanorods assembled microspheres, *Sens. Actuators B: Chem.* 140 (2) (2009) 514–519.
- [9] L. Parellada-Monreal, I. Castro-Hurtado, M. Martínez-Calderón, A. Rodríguez, S. Olaizola, D. Gamarra, J. Lozano, G. Mandayo, Study of sputtered ZnO modified by direct laser interference patterning: structural characterization and temperature simulation, *Appl. Surf. Sci.* 441 (2018) 331–340.
- [10] M. Bieda, E. Beyer, A.F. Lasagni, Direct fabrication of hierarchical microstructures on metals by means of direct laser interference patterning, *J. Eng. Mater. Technol.* 132 (3) (2010) 031015.
- [11] A.F. Lasagni, D.F. Acevedo, C.A. Barbero, F. Mücklich, One-step production of organized surface architectures on polymeric materials by direct laser interference patterning, *Adv. Eng. Mater.* 9 (1–2) (2007) 99–103.
- [12] M. Soldara, K. Taretto, J. Berger, A.F. Lasagni, Potential of photocurrent improvement in  $\mu$ -Si: H solar cells with TeO substrates structured by direct laser interference patterning, *Adv. Eng. Mater.* 18 (9) (2016) 1674–1682.
- [13] S. Ring, B. Stannowski, F. Fink, R. Schlattmann, Micro gratings written in ZnO: Al thin films using picosecond UV-laser interference patterning, *Phys. Status Solidi (RRL)-Rapid Res. Lett.* 7 (9) (2013) 635–638.
- [14] T. Roch, V. Weihnacht, H.-J. Scheibe, A. Roch, A.F. Lasagni, Direct laser interference patterning of tetrahedral amorphous carbon films for tribological applications, *Diamond Relat. Mater.* 33 (2013) 20–26.
- [15] L. Guo, H.-B. Jiang, R.-Q. Shao, Y.-L. Zhang, S.-Y. Xie, J.-N. Wang, X.-B. Li, F. Jiang, Q.-D. Chen, T. Zhang, H.-B. Sun, Two-beam-laser interference mediated reduction, patterning and nanostructuring of graphene oxide for the production of a flexible humidity sensing device, *Carbon* 50 (4) (2012) 1667–1673.
- [16] X. Chen, Y. Shen, W. Zhang, J. Zhang, D. Wei, R. Lu, L. Zhu, H. Li, Y. Shen, In-situ growth of ZnO nanowire arrays on the sensing electrode via a facile hydrothermal route for high-performance NO<sub>2</sub> sensor, *Appl. Surf. Sci.* 435 (2018) 1096–1104.
- [17] J.-S. Kim, J.-W. Yoon, Y.J. Hong, Y.C. Kang, F. Abdel-Hady, A. Wazzan, J.-H. Lee, Highly sensitive and selective detection of ppb-level NO<sub>2</sub> using multi-shelled WO<sub>3</sub> yolk-shell spheres, *Sens. Actuators B: Chem.* 229 (2016) 561–569.
- [18] L.S. Pilotto, R.M. Douglas, R.G. Attewell, S.R. Wilson, Respiratory effects associated with indoor nitrogen dioxide exposure in children, *Int. J. Epidemiol.* 26 (4) (1997) 788–796.
- [19] S.A. Abdul-Wahab, S.C.F. En, A. Elkamel, L. Ahmadi, K. Yetilmezsoy, A review of standards and guidelines set by international bodies for the parameters of indoor air quality, *Atmos. Pollut. Res.* 6 (5) (2015) 751–767.
- [20] J.M. Seguel, R. Merrill, D. Seguel, A.C. Campagna, Indoor air quality, *Am. J. Lifestyle Med.* 11 (4) (2017) 284–295.
- [21] I. Castro-Hurtado, T. Tavera, P. Yurrita, N. Pérez, A. Rodríguez, G.G. Mandayo, E. Casta no, Structural and optical properties of WO<sub>3</sub> sputtered thin films nanostructured by laser interference lithography, *Appl. Surf. Sci.* 276 (2013) 229–235 doi:10.1016/j.apsusc.2013.03.072.
- [22] G. Pawley, Unit-cell refinement from powder diffraction scans, *J. Appl. Crystallogr.* 14 (6) (1981) 357–361.
- [23] A. Le Bail, H. Duroy, J. Fourquet, Ab-initio structure determination of LiSbWO<sub>6</sub> by X-ray powder diffraction, *Mater. Res. Bull.* 23 (3) (1988) 447–452.
- [24] Bruker AXS GmbH, Karlsruhe, Germany, Bruker AXS. TOPAS 4-1, User Manual.
- [25] R.W. Cheary, A. Coelho, A fundamental parameters approach to X-ray line-profile fitting, *J. Appl. Crystallogr.* 25 (2) (1992) 109–121.
- [26] R.W. Cheary, A.A. Coelho, J.P. Cline, Fundamental parameters line profile fitting in laboratory diffractometers, *J. Res. Natl. Inst. Stand. Technol.* 109 (1) (2004) 1.
- [27] E.J. Mittemeijer, P. Scardi, *Diffraction Analysis of the Microstructure of Materials*, vol. 68, Springer Science & Business Media, 2013.
- [28] D. Balzar, Voigt-function model in diffraction line-broadening analysis, *Int. Union Crystallogr. Monogr. Crystallogr.* 10 (1999) 94–126.
- [29] J. Berger, T. Roch, S. Correia, J. Eberhardt, A.F. Lasagni, Controlling the optical performance of transparent conducting oxides using direct laser interference patterning, *Thin Solid Films* 612 (2016) 342–349.
- [30] P. Woodward, A. Sleight, T. Vogt, Ferroelectric tungsten trioxide, *J. Solid State Chem.* 131 (1) (1997) 9–17.
- [31] R. Diehl, G. Brandt, E. Saije, The crystal structure of triclinic WO<sub>3</sub>, *Acta Crystallogr. Sect. B* 34 (4) (1978) 1105–1111.

- [32] T. Vogt, P.M. Woodward, B.A. Hunter, The high-temperature phases of  $\text{WO}_3$ , *J. Solid State Chem.* 144 (1) (1999) 209–215.
- [33] E. Salje, The orthorhombic phase of  $\text{WO}_3$ , *Acta Crystallogr. Sect. B* 33 (2) (1977) 574–577.
- [34] W. Kehl, R. Hay, D. Wahl, The structure of tetragonal tungsten trioxide, *J. Appl. Phys.* 23 (2) (1952) 212–215.
- [35] H. Zheng, J.Z. Ou, M.S. Strano, R.B. Kaner, A. Mitchell, K. Kalantar-zadeh, Nanostructured tungsten oxide-properties, synthesis, and applications, *Adv. Funct. Mater.* 21 (12) (2011) 2175–2196.
- [36] I.M. Szilágyi, S. Saukko, J. Mizsei, A.L. Tóth, J. Madarász, G. Pokol, Gas sensing selectivity of hexagonal and monoclinic  $\text{WO}_3$  to  $\text{H}_2$ , *Solid State Sci.* 12 (11) (2010) 1857–1860.
- [37] G. Korotcenkov, The role of morphology and crystallographic structure of metal oxides in response of conductometric-type gas sensors, *Mater. Sci. Eng.: R: Rep.* 61 (1–6) (2008) 1–39.
- [38] M. Boulova, G. Lucazeau, Crystallite nanosize effect on the structural transitions of  $\text{WO}_3$  studied by Raman spectroscopy, *J. Solid State Chem.* 167 (2) (2002) 425–434.
- [39] C. Bundesmann, N. Ashkenov, M. Schubert, D. Spemann, T. Butz, E. Kaidashev, M. Lorenz, M. Grundmann, Raman scattering in  $\text{ZnO}$  thin films doped with Fe, Sb, Al, Ga, and Li, *Appl. Phys. Lett.* 83 (10) (2003) 1974–1976.
- [40] Y. Zou, Y. Zhang, D. Lou, H. Wang, L. Gu, Y. Dong, K. Dou, X. Song, H. Zeng, Structural and optical properties of  $\text{WO}_3$  films deposited by pulsed laser deposition, *J. Alloys Compd.* 583 (2014) 465–470.
- [41] V. Shapovalov, A. Komlev, V. Vit'ko, A. Zav'yalov, A. Lapshin, S. Moshkalev, V. Ermakov, Influence of annealing on the optical properties and chemical and phase compositions of tungsten-oxide films, *J. Surf. Invest. X-ray, Synchrotron Neutron Tech.* 10 (5) (2016) 1077–1086.
- [42] W. Wu, Q. Yu, J. Lian, J. Bao, Z. Liu, S.-S. Pei, Tetragonal tungsten oxide nanobelts synthesized by chemical vapor deposition, *J. Cryst. Growth* 312 (21) (2010) 3147–3150.
- [43] M.-W. Ahn, K.-S. Park, J.-H. Heo, J.-G. Park, D.-W. Kim, K.J. Choi, J.-H. Lee, S.-H. Hong, Gas sensing properties of defect-controlled  $\text{ZnO}$ -nanowire gas sensor, *Appl. Phys. Lett.* 93 (26) (2008) 263103.
- [44] W. An, X. Wu, X.C. Zeng, Adsorption of  $\text{O}_2$ ,  $\text{H}_2$ ,  $\text{CO}$ ,  $\text{NH}_3$ , and  $\text{NO}_2$  on  $\text{ZnO}$  nanotube: a density functional theory study, *J. Phys. Chem. C* 112 (15) (2008) 5747–5755.
- [45] M. Chen, Z. Wang, D. Han, F. Gu, G. Guo, High-sensitivity  $\text{NO}_2$  gas sensors based on flower-like and tube-like  $\text{ZnO}$  nanomaterials, *Sens. Actuators B: Chem.* 157 (2) (2011) 565–574.
- [46] Y. Qin, Z. Ye, DFT study on interaction of  $\text{NO}_2$  with the vacancy-defected  $\text{WO}_3$  nanowires for gas-sensing, *Sens. Actuators B: Chem.* 222 (2016) 499–507.
- [47] G. Sakai, N. Matsunaga, K. Shimano, N. Yamazoe, Theory of gas-diffusion controlled sensitivity for thin film semiconductor gas sensor, *Sens. Actuators B: Chem.* 80 (2) (2001) 125–131.
- [48] F. Oudrhiri-Hassani, L. Presmanes, A. Barnabe, P. Tailhades, Microstructure, porosity and roughness of RF sputtered oxide thin films: characterization and modelization, *Appl. Surf. Sci.* 254 (18) (2008) 5796–5802.
- [49] J. Li, Y. Lu, Q. Ye, C. Martin, J. Han, M. Meyyappan, Carbon nanotube sensors for gas and organic vapor detection, *Nano Lett.* 3 (7) (2003) 929–933.
- [50] T. Kida, A. Nishiyama, Z. Hua, K. Suematsu, M. Yuasa, K. Shimano,  $\text{WO}_3$  nanolamella gas sensor: porosity control using  $\text{SnO}_2$  nanoparticles for enhanced  $\text{NO}_2$  sensing, *Langmuir* 30 (2014) 2571–2579.
- [51] M. Epifani, J.D. Prades, E. Comini, E. Pellicer, M. Avella, P. Siciliano, G. Faglia, A. Cirera, R. Scotti, F. Morazzoni, et al., The role of surface oxygen vacancies in the  $\text{NO}_2$  sensing properties of  $\text{SnO}_2$  nanocrystals, *J. Phys. Chem. C* 112 (49) (2008) 19540–19546.
- [52] M. Hjiri, L. El Mir, S.G. Leonardi, N. Donato, G. Neri,  $\text{CO}$  and  $\text{NO}_2$  selective monitoring by  $\text{ZnO}$ -based sensors, *Nanomaterials* 3 (3) (2013) 357–369.
- [53] B. Xiao, D. Wang, F. Wang, Q. Zhao, C. Zhai, M. Zhang, Preparation of hierarchical  $\text{WO}_3$  dendrites and their applications in  $\text{NO}_2$  sensing, *Ceram. Int.* 43 (11) (2017) 8183–8189.
- [54] Y.-K. Chung, M.-H. Kim, W.-S. Um, H.-S. Lee, J.-K. Song, S.-C. Choi, K.-M. Yi, M.-J. Lee, K.-W. Chung, Gas sensing properties of  $\text{WO}_3$  thick film for  $\text{NO}_2$  gas dependent on process condition, *Sens. Actuators B: Chem.* 60 (1) (1999) 49–56.
- [55] N. Yamazoe, K. Shimano, Theory of power laws for semiconductor gas sensors, *Sens. Actuators B: Chem.* 128 (2) (2008) 566–573.
- [56] P. Lantto, V.L.S. Romppainen, A study of the temperature dependence of the barrier energy in porous tin dioxide, *Sens. Actuators* 14 (2) (1998) 149–163.
- [57] J. Samà, S. Barth, G. Domènech-Gil, J.-D. Prades, N. López, O. Casals, I. Gràcia, C. Cané, A. Romano-Rodríguez, Site-selectively grown  $\text{SnO}_2$  NWs networks on micromembranes for efficient ammonia sensing in humid conditions, *Sens. Actuators B: Chem.* 232 (2016) 402–409.
- [58] S.-C. Chang, Oxygen chemisorption on tin oxide: correlation between electrical conductivity and EPR measurements, *J. Vac. Sci. Technol.* 17 (1) (1980) 366–369.
- [59] M. Gillet, C. Lemire, E. Gillet, The role of surface oxygen vacancies upon  $\text{WO}_3$  conductivity, *Surf. Sci.* 532–535 (2) (2003) 519–525.

**Laura Parellada Monreal** received her BS degree in Physics from the University of Barcelona in 2013 and her MSc degree in Nanophysics and Nanostructures from the University Joseph Fourier in Grenoble (France) in 2015. Since 2016, she is a PhD student in the Micro and Nano Systems Research Line. Her PhD project is focused on semiconductor materials nanostructured by laser techniques for gas sensing on environmental applications.

**Sandro Gherardi** received his Bachelor's Degree in Tecnologie Fische Innovative (TFI) in

2002, with a thesis addressed to the study of the electrical response to various pollutant gases, based on nanostructured gas sensors and performed at the Sensors and Semiconductors Laboratory of the Department of Physics and Earth Sciences of University of Ferrara, where is today employed as assistant engineer. He continues to deal with environmental/industrial sensors, conducting researches on semiconductor materials for solid state sensors, installation of environmental monitoring and industrial control units, optimization and implementation of compressed gas transmission lines, in various programming languages and communication interfaces with laboratory equipment. From September 2016 is employed as IT manager at SCENT S.r.l.

**Giulia Zonta** received the Bachelor's Degree in Physics and Astrophysics in December 2010 (110/110 cum laude) and the Master's Degree in Physics in October 2013 (110/110), at the University of Ferrara. In April 2017, she received her Ph.D. in Matter Physics, working with the Sensors Team, coordinated by Prof. Cesare Malagù. Currently her postdoc research focuses on the study of the physico-chemical behaviour of chemoresistive nanostructured gas sensors put in contact with volatile organic compounds (VOCs) of medical interest. She is the Sales Executive and co-founder of the start-up SCENT S.r.l, with the aim to create prototypes for tumour preventive screening and monitoring and with SCENT team, she won diverse competitions as Premio Marzotto 2015.

**Cesare Malagù** was born in 1974 in Ferrara, Italy. He received a degree in Physics at the University of Ferrara in 1997 (Summa Cum Laude) and the Ph.D. in experimental physics in 2001. He has been teaching General Physics since 2001 and has been a Lecturer since 2007. His research activity is based on modelling of transport phenomena in nanostructured semiconductors. His expertise regards thick-film gas sensors applied to environmental monitoring and cancer screening. He has 75 papers in peer-reviewed journals (Hirsch index 29) and numerous proceedings and invited lectures; moreover, he is in the editorial board of several journals. He has been coordinating the sensors group at the University of Ferrara since 2010 and he is an associate professor since 2016.

**Davide Casotti** Bachelor in Geology at the University of Ferrara in 2010. He got his Ph.D. in 2017 in Physic and Nanosciences at University of Modena and Reggio Emilia. Research activity has focused on nanomaterials (powders and thin films), gas sensors, and monocrystals characterization.

**Giuseppe Cruciani** is Full Professor of Mineralogy at the Department of Physics and Earth Sciences, University of Ferrara. Graduate with honour in Geological Sciences in 1989 at the University of Perugia where he got a PhD in Mineralogy (Crystallography) and Petrology in 1993. Visiting scientist in 1995 at the European Synchrotron Radiation Facility (ESRF) in Grenoble, France, there he served in the chemistry review committee for project selection from 2008 to 2010. Since 2016 is Chair of proposal review panel for hard condensed matter-structures at the Elettra synchrotron in Trieste, Italy. Past President 2012–2013 of the Italian Society of Mineralogy and Petrology, is currently (2016–2019) President of the Italian Zeolite Association. Serves as Associate Editor of the European Journal of Mineralogy. Major research fields in crystallography and crystal-chemistry of microporous materials and oxide systems for wide application fields. Experimental skills mostly focused on single crystal and powder diffraction, both with conventional X-rays and large scale facility radiation (synchrotron X-rays and neutrons). Author of about 150 articles in international journals and more than 10 book chapters, with 2795 citations, his H-index is equal to 30 (January 2019).

**Vincenzo Guidi** Co-founder in 1996 of the Sensors and Semiconductors Lab (SSL) at Ferrara University with the aim to study nano-phased metal oxides for gas sensing via chemo-resistive effect. In particular, he studied the correlation existing between gassensitivity of films vs. structural features of the sensing materials. It was pursued the investigation of novel materials for gas sensing and some methods for their deposition were established. Information on basic sensing mechanisms and on grain coalescence in metal-oxides were found out as well as new methods for grain-growth inhibition. He deepened the understanding of gas sensing also from the theoretical standpoint. Some models highlighting the effects of small dimensionality of nanograins and their correlation to the gas-sensing qualities were put forward. He has been organiser of national and international projects and events on chemical sensors and actively played editorial roles. Professor since 2006, he is currently Director of the Department of Physics and Earth Sciences of Ferrara University.

**Miguel Martínez Calderón** received his bachelor degree in Materials Engineering from Polytechnique University of Madrid in 2013. He also obtained a Master's degree in Biomedical Engineering from the same university in 2014. In May 2018, he received his Ph.D in applied engineering working with the Additive Manufacturing and Laser group of CEIT, in the Materials & Manufacturing division. Currently he works at the same institution as a junior researcher and his work is focused on the development of advanced functional surfaces based on ultrafast laser technology and its application. His research interest includes ultrafast processes in materials, micro and nano structuring of materials surfaces, development of advanced surfaces applications and phenomena related to the interaction of light with matter in the micro/nano scale.

**Irene Castro Hurtado** received her BS degree in Physics from the University of the Basque Country in 2008 and her PhD degree in Physics from the University of Navarra, San Sebastián, in 2011. In 2008, she joined Ceit-IK4 as a researcher of the Sensors & Analog Electronics Group, focusing her work on industrial monitoring applications. Her main research interests are in the field of materials science, solid state physics and micro and nanotechnology. She joined CIC Energigune in 2017 as a postdoc for developing solid state batteries for industrial projects. Since 2018, she works at Tubacex as metallurgy responsible for the Quality department. She is author or co-author of more than 15

scientific papers in peer-reviewed international journals and more than 20 presentations at international conferences. She has been lecturer of Materials Science and Fabrication of Electronics Systems at Tecnun, Engineering School of the University of Navarra from 2008 to 2017.

**Daniel Gamarra** received the Degree in Chemistry in 2003 from University of Granada, Spain and Ph.D. degree in 2008 from Universidad Autonoma de Madrid, Spain. He has worked in Nanostructured Catalysts for Energy department of Instituto de Catalisis y Petroleoquimica (CSIC) in new catalytic systems based in copper and cerium mixed for CO preferential oxidation in hydrogen rich current (application in PEM fuel cells) and for anode systems in SOFC fuel cells. His Post Ph.D. working was carried out in the same place about new catalytic supports of Cerium oxide with exposure of thermodynamically unstable faces for preferential CO oxidation and hydrothermal synthesis method of new materials sulphured for solar cells applications. His actual career is associated to Manager Technician in solid and surface characterization analytic service in University of Extremadura and "ICTs NANBIOSIS" (Spanish singular scientific technical installation). His research interests include new advances in surface characterization by TOF-SIMS, XPS and other technics.

**Jesús Lozano** received the B. Sc. degree in Electronic Engineer in 2001 and Ph. D. degree in 2005 from Universidad Complutense de Madrid, Spain. He has worked in instrumentation systems at Electronics Department of the University Complutense of Madrid, in chemical sensors and electronic noses at the Laboratorio de Sensores, Consejo Superior de Investigaciones Científicas (CSIC), Madrid, in control, modelling and simulation at Naval Engineering School of Universidad Politécnica de Madrid. Presently, he works as associate professor at the Industrial Engineering School of Universidad de Extremadura, Badajoz. His research interests include gas sensors, instrumentation and

measurement systems, and pattern recognition techniques.

**Lionel Presmanes** received his PhD degree, for his thesis-work on ferrite thin films for magneto-optical storage. Since 1997, he has been working in CIRIMAT laboratory at University Paul Sabatier (Toulouse) and he is also CNRS researcher since 2001. His research interests are focused on the preparation of sputtered oxide and nanocomposites thin films and the study of their microstructure as well as their electrical, magnetic and optical properties. He developed sputtered ferrite thin films to be integrated as sensitive layers in magneto-optical disks and micro-bolometers (IR sensors). His work is currently focused on transparent conducting oxides, thermoelectric oxide layers and semiconductor sensitive layers for gas sensors.

**Gemma Garcia Mandayo** (PhD, female) is a Researcher and Project Manager in the Information and Communications Technology Division of Ceit-IK4 (Research Institute in San Sebastian, Spain) and Professor and Director of the Master in Telecommunication Engineering at Tecnun, Engineering School of the University of Navarra. She obtained her Degree in Electronics Engineering (1996) and her Doctorate (2002) from the University of Navarra. Her main research and technical interests are in the field of micro and nano-system technology applied to sensing devices for industrial and environmental applications, focusing on the development of innovative sensor solutions. She has participated in 32 national and international research projects, 9 of them as main researcher and 5 as coordinator, with mainly an applied research scope. She has supervised three doctoral theses and is author or co-author of 25 scientific contributions in peer-reviewed journals and more than 50 international conferences of relevance in the Microelectronics and Sensors fields (7 invited conferences and 21 oral contributions). She is an active referee of the scientific publishing houses Elsevier, Wiley and MDPI Online and evaluator of scientific projects for public agencies such as ANEP in Spain and the European Commission.